REGULAR ARTICLE

blood advances

Tumor microenvironment of Burkitt lymphoma: different immune signatures with different clinical behavior

Maria Chiara Siciliano,[1,*] Giorgio Bertolazzi,[2,3,*] Gaia Morello,[2] Salvatore Tornambè,[1] Marcello Del Corvo,[4] Massimo Granai,[1] Maria Rosaria Sapienza,[4] Ciara I. Leahy,[5] Eanna Fennell,[5] Beatrice Belmonte,[2] Felice Arcuri,[1] Margherita Vannucchi,[1] Virginia Mancini,[1] Raffaella Guazzo,[1] Roberto Boccacci,[1] Noel Onyango,[6] Joshua Nyagol,[7] Raffaella Santi,[8] Gioia Di Stefano,[8] Domenico Ferrara,[1] Cristiana Bellan,[1] Teresa Marafioti,[9] German Ott,[10] Reiner Siebert,[11] Leticia Quintanilla-Fend,[12] Falko Fend,[12] Paul Murray,[5] Claudio Tripodo,[5,13] Stefano Pileri,[4] Stefano Lazzi,[1] and Lorenzo Leoncini[1]

[1]Department of Medical Biotechnologies, University of Siena, Siena, Italy; [2]Tumor Immunology Unit, Department of Health Sciences and [3]Department of Economics, Business, and Statistics, University of Palermo, Palermo, Italy; [4]Istituto Europeo di Oncologia (IEO), IRCSS Milano, Milan, Italy; [5]School of Medicine, Bernal Institute, Health Research Institute and Limerick Digital Cancer Research Centre, University of Limerick, Limerick, Ireland; [6]Department of Medical Microbiology and Immunology, and [7]Department of Human Pathology, University of Nairobi, Nairobi, Kenya; [8]Department of Pathology, University of Florence, Florence, Italy; [9]Department of Cellular Pathology, University College London, London, United Kingdom; [10]AbteilungfürKlinischePathologie, Robert-Bosch-Krankenhaus and Dr. Margarete Fischer-Bosch InstitutfürKlinischePharmakologie, Stuttgart, Germany; [11]Institute of Human Genetics, Ulm University and Ulm University Medical Center, Ulm, Germany; [12]Institut für Pathologie und Neuropathologie, University of Tubingen, Tubingen, Germany; and [13]Tumor and Microenvironment Histopathology Unit, IFOM, the FIRC Institute of Molecular Oncology, Milan, Italy

Key Points

- BL with granulomatous reaction was characterized by an M1 signature and *INFG* in $CD8^+$ cells, whereas BL with starry sky showed M2 genes.
- Tumor-associated macrophages repolarization and epigenetic regulators may open new therapeutic options for the fight against BL lymphoma.

Burkitt lymphoma (BL) is characterized by a tumor microenvironment (TME) in which macrophages represent the main component, determining a distinct histological appearance known as "starry sky" pattern. However, in some instances, BL may exhibit a granulomatous reaction that has been previously linked to favorable prognosis and spontaneous regression. The aim of our study was to deeply characterize the immune landscape of 7 cases of Epstein-Barr virus–positive (EBV^+) BL with granulomatous reaction compared with 8 cases of EBV^+ BL and 8 EBV-negative (EBV^-) BL, both with typical starry sky pattern, by Gene expression profiling performed on the NanoString nCounter platform. Subsequently, the data were validated using multiplex and combined immunostaining. Based on unsupervised clustering of differentially expressed genes, BL samples formed 3 distinct clusters differentially enriched in BL with a diffuse granulomatous reaction (cluster 1), EBV^+ BL with typical starry sky pattern (cluster 2), EBV^- BL with typical "starry sky" (cluster 3). We observed variations in the immune response signature among BL with granulomatous reaction and BL with typical "starry sky," both EBV^+ and EBV^-. The TME signature in BL with diffuse granulomatous reaction showed a proinflammatory response, whereas BLs with "starry sky" were characterized by upregulation of M2 polarization and protumor response. Moreover, the analysis of additional signatures revealed an upregulation of the dark zone signature and epigenetic signature in BL with a typical starry sky. Tumor-associated macrophages and epigenetic regulators may be promising targets for additional therapies for BL lymphoma, opening novel immunotherapeutic strategies.

Submitted 22 August 2023; accepted 29 May 2024; prepublished online on *Blood Advances* First Edition 11 June 2024; final version published online 15 August 2024. https://doi.org/10.1182/bloodadvances.2023011506.

*M.C.S. and G.B. contributed equally to this study.

Data are available on request from coauthor, Maria Chiara Siciliano (siciliano10@student.unisi.it).

The full-text version of this article contains a data supplement.

Introduction

The tumor microenvironment (TME) in B-cell lymphomas is highly variable in terms of spatial arrangement and the type of inflammatory cells, blood and lymphatic vascular networks, and extracellular matrix.[1] Growing evidence suggests that TME plays an important role in various processes, including the development and dissemination of B-cell lymphomas.[2,3] In aggressive lymphomas, particularly Burkitt lymphoma (BL), owing to their high proliferation rate, intensive chemotherapy is the standard of care. Unfortunately, these treatments are not as effective in the older patients who are immunocompromised and in the equatorial African population, in which BL is the most common childhood cancer.[4,5] Having a complete understanding of TME biology in BL and the way in which lymphoma cells interact with TME can truly make all the difference when it comes to developing new target therapies and tumor prognosis prediction. Certainly, research in the field of lymphomas is highly complex and multifaceted, and there is still much to learn. However, with continued exploration and innovative thinking, there is a strong hope for improved outcomes for those affected by BL and other lymphomas. BL is a type of lymphoma that has been historically divided into 3 categories: endemic , sporadic , and immunodeficiency associated. However, these factors are tightly confounded by the presence or absence of Epstein-Barr virus (EBV). Thus, the most recent developments in BL biology have prompted the fifth edition of the World Health Organization classification of hematolymphoid tumors to recommend distinguishing EBV-positive (EBV^+) and EBV-negative (EBV^-) BL, based on their molecular features regardless of the epidemiological context and geographic location.[6,7] At the histological level, BL shows macrophages with abundant cytoplasm dispersed in the background of a monomorphic population of rapidly proliferating B cells with basophilic cytoplasm. Reactive infiltrating lymphocytes are few, whereas scattered phagocytic macrophages give rise to the characteristic histological aspect of BL, known as the "starry sky" appearance.[8] These macrophages, along with mesenchymal stem cells, stromal cells, and soluble factors, represent the main components of the TME of BL. The role of macrophages in BL tumor-associated macrophages (TAMs) is not fully understood, but they may contribute to tumor advancement by secreting chemokines and cytokines.[9,10] Over the last 2 decades, different macrophage polarizations have been recognized as increasingly relevant for lymphomagenesis, contributing to the effects of the immune microenvironment.[11,12] A constructive model inspired by T helper 1 (Th1) vs Th2 nomenclature has been developed to describe the complex mechanism of macrophage activation as polarization toward 2 opposite states: M1 with proinflammatory properties and M2 with protumoral properties. M1 macrophages produce proinflammatory cytokines which boost cancer immunosurveillance and cytotoxicity.[13,14] However, these effects are counterbalanced by M2 macrophages with the anti-inflammatory and protumoral effects. Interestingly, there are some cases of BL that are characterized by conspicuous granulomatous reactions. These reactions can make detection of neoplastic proliferation difficult. Usually, these cases are EBV^+ and tend to occur in the early stage of the disease, showing at times spontaneous regression without therapy.[15-19] Macrophages in granulomas are derived both from circulating monocytes attracted by chemotaxis and from local resident macrophages recruited by T-cell–derived growth factors. $CD4^+$ T cells accumulate in the center of epithelioid granulomas, whereas most $CD8^+$ T cells are found at their periphery. Recent data have shown, using multiplex immunohistochemistry, that the TME of BL with granulomatous reaction is characterized by the prevalence of M1 macrophages and Th1 lymphocytes with a proinflammatory response, which may explain the spontaneous regression of such cases.[19] Still, the differences in the composition of the cellular and soluble components of the BL TME in patients with both EBV^+ and EBV^- remain unclear. Therefore, the aim of this study was to delve deeper into the immune landscape of BL in 7 cases of EBV^+ BL with granulomatous reaction compared with 8 cases of EBV^+ BL and 8 BL EBV^-, both with typical starry sky patterns, by applying NanoString technologies, focusing on the immune gene categories using a large panel of immune-related genes.

Materials and methods

Case selection

Formalin-fixed paraffin-embedded (FFPE) BL samples were obtained from the Department of Medical Biotechnologies (University of Siena, Siena, Italy), the Pathology section of the University of Florence (Florence, Italy), and the University of Nairobi (Nairobi, Kenya). The diagnosis of BL was made by hematopathology experts, who followed the essential criteria reported in the fifth edition of the World Health Organization classification of hematolymphoid tumors. Diagnostic immunohistochemistry was performed using a large panel of antibodies including CD20, CD10, BCL6, and LMO2. BCL2, Myc, and Ki67 on the Ventana BenchUltra (Roche Diagnostics, Monza, Italia), according to the manufacturer's instructions. To assess the presence of EBV, in situ hybridization for EBV-encoded small RNAs was performed on all FFPE cases, cut at 5 µm, using an automated staining system (Ventana BenchMark ULTRA, Roche Diagnostics), as previously described[10]. Fluorescence in situ hybridization analysis for *MYC* rearrangement (Vysis MYC Dual Color Break Apart Rearrangements Probe; Abbott, Wiesbaden, Germany), translocation t (8;14) (q24;q32) (MYC::IgH, ZytoVision GmbH, Bremerhaven, Germany), and MYC::IgL (probes kindly provided by the Institute of Human Genetics, Ulm University Medical Center, Ulm, Germany) was performed for each case. *BCL6* and *BCL2* rearrangements were investigated in each case using respective break apart probes (Vysis BCL2 or BCL6 Dual Color Break Apart Rearrangements Probe; Abbott, Wiesbaden, Germany) according to the manufacturer's instructions. Furthermore, aberrations on the long arm of chromosome 11q were evaluated using fluorescence in situ hybridization analysis (ZytoLight SPEC 11q gain/loss Triple Color Probe).[19]

Immune-related GEP using the NanoString platform. Digital multiplexed gene expression profiling (GEP) of 730 immune-related genes and 40 housekeeping genes was performed using the nCounter PanCancer Immune Profiling Panel (NanoString Technologies, Seattle, WA) on primary diagnostic FFPE tumor tissue.[20] Total RNA from 23 FFPE 10 µm thick sections from each diagnostic sample was isolated using the RNeasy FFPE kit (Qiagen, Hilden, Germany). The protocol included deparaffinization, proteinase K digestion, extraction, elution, or hydration procedures, and DNase treatment to obtain DNase-free RNA. RNA concentration was measured using the Qubit RNA HS Assay Kit following the manufacturer's instructions.

Bioinformatics and data analysis

Raw expression data were analyzed using the NanoStringNorm R package for background correction and between-sample normalization. Normalized data were then used to perform and plot principal component analysis (PCA) with the FactoMine and ggplot2 R packages, respectively. For hierarchical clustering analysis, the Euclidean distance metric across samples was considered for building trees within the pheatmap package. Differential expression analyses were carried out using the Bioconductor package limma and considering pairwise comparisons between different BL subtypes.[21,22] We applied the voom[21] method to model the mean-variance relationship, after which lmFit was used to fit per-gene linear models, and empirical Bayes moderation was applied with the eBayes function. Upregulated or downregulated genes were selected for subsequent analysis if their expression values were found to exceed an adjusted *P* value cutoff of <.05, after multiple testing corrections using a moderated *t* statistic.[22] Genes differentially expressed were considered statistically significant when the adjusted *P* value (false discovery rate [FDR]) was <.05. Gene set enrichment analysis (GSEA) was performed using the gsea[23] function of the phenoTest R package[24] to test the association between the predefined groups of genes and BL subtypes. The gene lists used for this analysis were derived from KEGG and Reactome databases,[25] of which only gene sets represented in the nCounter PanCancer Immune Profiling Panel were included in the computation. The output of GSEA is an enrichment score, a normalized enrichment score that accounts for the size of the gene set being tested, a *P* value, and an estimated FDR. Computing NES, *P* values and FDR requires a permutation-based approach, for which we computed 10 000 permutations. Heat maps were used for gene pathway representation. Additional pathways of interest were considered using the NanoString Panel Pro tool (https://nanostring.com/products/ncounter-assays-panels/panel-selection-tool/). The Kruskal-Wallis (nonparametric analysis of variance) test was used to identify pathways whose genes were associated with the BL groups. The heat map vertical bars indicate the significance of the Kruskal-Wallis *P* values. CIBERSORTx software was used to estimate the immune deconvolution fractions.[26] The immune deconvolution fractions were compared between EBV$^+$ BL with granulomatous reaction and BL with typical "starry sky" (both EBV$^+$ and EBV$^-$) using the Mann-Whitney nonparametric rank test, instead of the unpaired *t* test, because the data could not be assumed to be normally distributed. Bioinformatics and statistical analyses were performed using R statistical software (v4.3.0; http://www.R-project.org)[27,28] (a detailed description of bioinformatic analysis is provided in the supplemental Data).

Table 1. Clinical pathological features of BL clusters

Case	Sex	Age, y	Ethnicity	Location	Stage	EBV status	Response to therapy	Cluster	
BL1	M	10	African	Lymph node	II	Pos	Complete remission	Cluster 1	5 BL EBV$^+$ with diffuse granulomatous reaction
BL2	F	65	Caucasian	Lymph node	I	Pos	Spontaneous regression		
BL3	F	26	Caucasian	Oral cavity	II	Pos	Complete remission		
BL4	M	12	African	Oral cavity	I	Pos	Spontaneous regression		
BL5	F	47	Caucasian	Lymph node	I	Pos	Spontaneous regression		
BL6	M	9	African	Lymph node	III	Pos	Complete remission	Cluster 2	5 BL EBV$^+$ with typical starry sky
BL7	M	70	Caucasian	Na	III	Pos	Complete remission		
BL8	F	9	African	Abdominal mass	III	Pos	Complete remission		
BL9	M	3	African	Na	II	Pos	Complete remission		
BL10	F	8	African	Gastro intestinal tract	II	Pos	Complete remission		
BL11	F	5	Caucasian	Gastro intestinal tract	III	Neg	Complete remission	Cluster 3	8 BL EBV$^-$ with typical starry sky, 3 BL EBV$^+$ with typical starry sky, and 2 BL EBV$^+$ with partial granulomatous reaction
BL12	M	11	Caucasian	Oral mucosa	II	Neg	Complete remission		
BL13	M	8	Caucasian	Gastro intestinal tract	III	Neg	Complete remission		
BL14	M	6	Caucasian	Gastro intestinal tract	III	Neg	Complete remission		
BL15	M	50	Caucasian	Bone marrow	IV	Neg	Relapse		
BL16	M	14	Caucasian	Abdominal mass	III	Neg	Complete remission		
BL17	M	8	Caucasian	Oral mucosa	II	Neg	Complete remission		
BL18	F	6	Caucasian	Na	III	Neg	Remission		
BL19	M	12	African	Na	III	Pos	Not available		
BL20	F	63	Caucasian	Na	II	Pos	Not available		
BL21	M	7	African	Na	III	Pos	Not available		
BL22	F	10	African	Na	II	Pos	Complete remission		
BL23	F	4	African	Abdominal mass	II	Pos	Complete remission		

Cluster 1 consisted of the 5 BL with a diffuse granulomatous reaction, including 3 of 5 cases with spontaneous regression, whereas cluster 2 had 5 EBV$^+$ BL with typical starry sky pattern, and cluster 3 includes 8 EBV$^-$ BL with typical starry sky, 2 cases of BL with a partial granulomatous reaction, and 3 cases of EBV$^+$ BL with typical starry sky.

F, female; M, male, Na, not available; neg, negative; pos, positive; BL, Burkitt Lymphoma

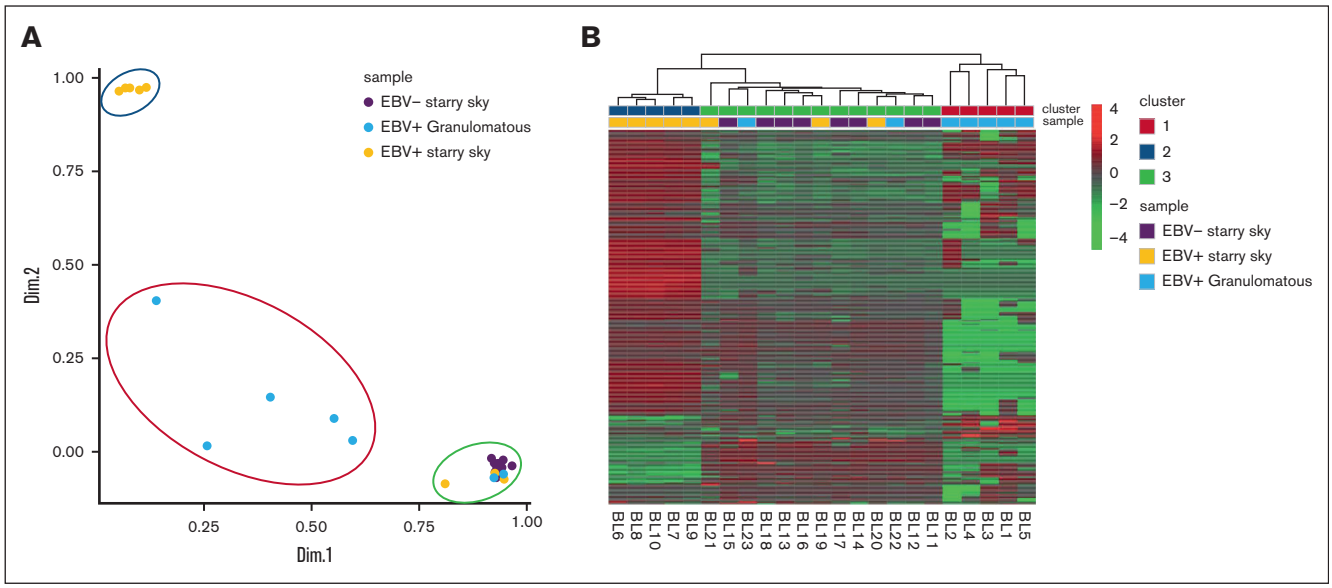

Figure 1. PCA and heat map showed 3 clusters of BL. PCA (A) and heat map (B) revealed the presence of 3 distinct clusters. Cluster 1 consisted of the 5 BL with a diffuse granulomatous reaction (blue), cluster 2 had 5 EBV$^+$ BL with typical starry sky pattern (orange), and cluster 3 includes 8 EBV$^-$ BL with typical starry sky (violet), 2 cases of BL with a partial granulomatous reaction, and 3 cases of EBV$^+$ BL with typical starry sky. Heat map visualizing the expression levels of immune-related genes (rows) in each BL sample (column). Upregulated or downregulated genes were selected for subsequent analysis if their expression values were found to exceed an adjusted *P* value cutoff of <.05, after multiple testing correction using a moderated *t* statistic.

In situ messenger RNA (mRNA) hybridization and immunolocalization analyses

The human Interferon Gamma (IFNG) probe hybridization (Cod. 310501) was performed using the RNAscope 2.5 HD Detection Reagent-BROWN (Advanced Cell Diagnostic) in accordance with the manufacturer's protocol. For multiple-marker immunostaining, the tissue section was subjected to sequential rounds of single-marker immunostaining, and the binding of the primary antibodies was revealed by fusing specific secondary antibodies conjugated with different enzymes (a detailed description of in situ hybridization is provided in supplemental Data[29,30]).

Multiplex immunostaining

Four-micrometers-thick human sections were deparaffinized, rehydrated, and unmasked using Novocastra Epitope Retrieval Solutions pH 9 in a thermostatic bath at 98°C for 30 minutes. Subsequently, sections were brought to room temperature and washed with phosphate-buffered saline. After Fc blocking by a specific protein block (Novocastra), the samples were incubated with primary antibodies against CD206 (1:4000 pH 9; Abcam), CD163 (clone 10D6, 1:100 Ph6; Novocastra), and CD68 (clone KP1, 1:50 pH 9; Dako), and the binding of the primary antibodies was revealed using specific secondary antibodies conjugated with different fluorophores anti-mouse and anti-rabbit (Alexa Fluor 488 and 568 conjugates). The slides were analyzed under a Zeiss Axioscope A1 microscope equipped with 4 fluorescence channels with widefield IF. Microphotographs were collected using a Zeiss Axiocam 503 color digital camera with Zen 2.0 software (Zeiss). Quantitative analyses of immunofluorescence staining were performed by calculating the average percentage of positive cells in 5 nonoverlapping fields at medium-power magnification (×200) using HALO image analysis software (v3.2.1851.229, Indica Labs). To gain a better understanding of macrophage polarization in our cohort, we applied multiplex immunofluorescence (mIF) to FFPE BL cases with granulomatous reactions. Recent studies have indicated that C-Maf is a specific marker for M2 macrophages[10] (a detailed description of mIF is provided in the supplemental Data).

SOPHiA DDM Lymphoma Solution

DNA library preparation was performed using the SOPHiA DNA Library Prep Kit II (SOPHiA GENETICS, Lausanne, Switzerland), covering 73 lymphoma-related genes (a detailed description of Next Generation Sequencing [NGS] is provided in the supplemental Data).

All procedures performed in this study involving human participants were in accordance with the ethical standards of the institutional research committee and with the 1964 Declaration of Helsinki and its later amendments or comparable ethical standards. This was a noninterventional study of archived tissue samples.

Results

Patient information

The case cohort comprised 10 females and 13 males, ranging in age from 5 to 70 years. Anatomical localization included the gastrointestinal tract, oral mucosa, bone marrow, lymph nodes, and abdominal mass. We analyzed 3 groups of BLs composed of 8 EBV$^-$ BL with starry sky pattern, 8 EBV$^+$ BL with starry sky pattern, and 7 BL with granulomatous reaction. Among the latter, 5 of 7 cases were characterized by a diffuse granulomatous reaction that partially obscured neoplastic proliferation and 2 of 7 cases were characterized by a partial granulomatous reaction. The cases with granulomatous reactions were stage I/II and 3 of the 7 cases showed spontaneous regression. Two patients were in complete

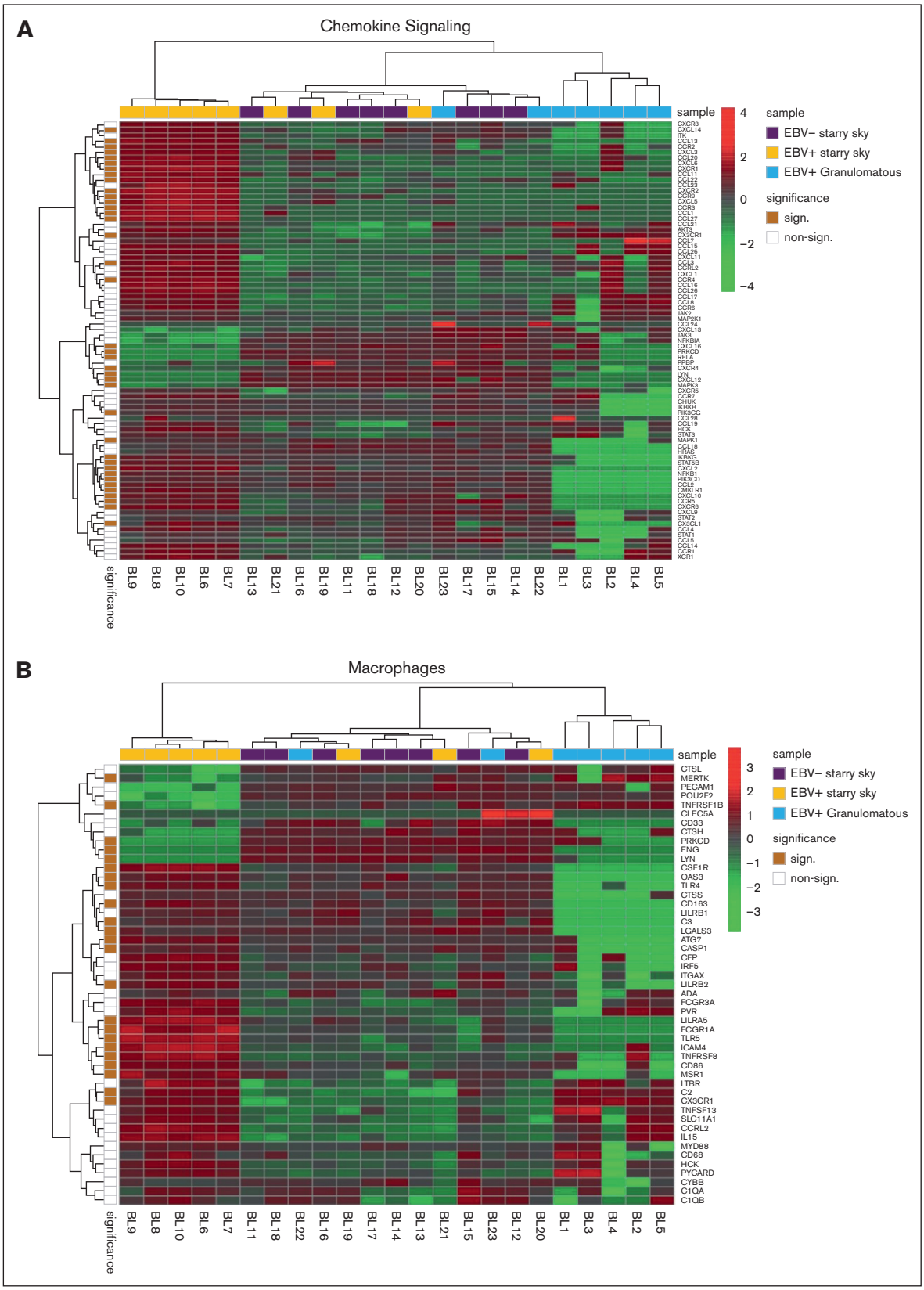

Figure 2. Immune differences between BL with granulomatous reaction and BL with typical starry sky. GEP showed that BL with typical starry sky pattern both EBV^{+} (orange) and EBV^{-} (violet) were enriched in and M2-related chemokines (A), M2 macrophages (B), and immune exhaustion signature (C).

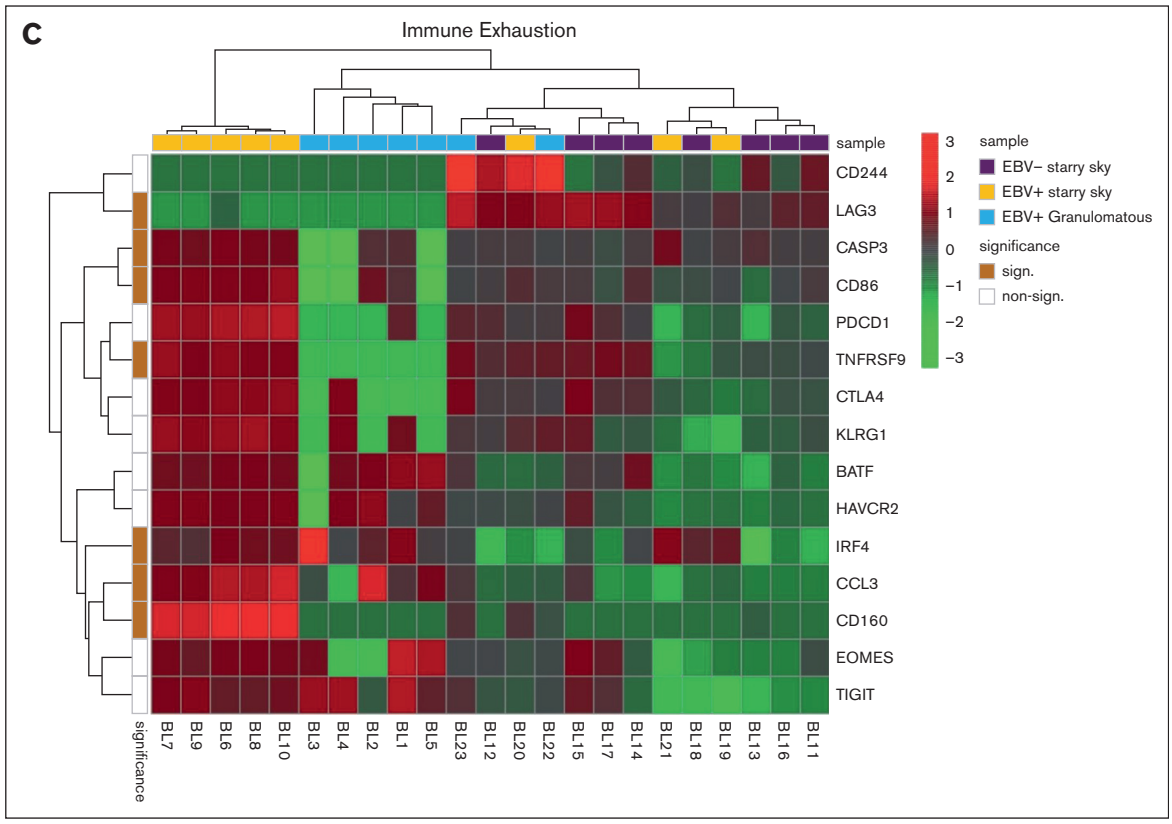

Figure 2 (continued)

remission after 5 years of treatment 19, whereas 1 case was lost to follow-up after 3 years. In contrast, cases with typical starry sky, EBV$^+$ or EBV$^-$, were mainly stage III or IV, with bulky disease, significantly different from cases with granulomatous reaction ($P <$ .001; Table 1). The diagnosis of BL was issued by expert hematopathologists. All the cases had typical morphology and immunophenotype features of BL (CD20$^+$, CD10$^{+,}$ BCL6$^+$, LMO2$^-$, BCL2$^-$, Myc >80%, and Ki67 >95%) and were harbored in 21 of 23 cases of IGH::MYC translocation, and 2 of the 20 IGL::MYC translocation demonstrated using fusion fluorescence in situ hybridization. *BCL2* and *BCL6* rearrangement and 11q aberration were not detected.

PCA and heat map graph identify 3 groups of BL

The NanoString panel analysis included all 23 BL FFPE samples that satisfied the RNA quality criteria. PCA and heat map graph revealed the presence of 3 distinct clusters (Figure 1A-B). Specifically, cluster 1 consisted of 5 BL with a diffuse granulomatous reaction, including 3 of 5 cases with spontaneous regression. Cluster 2 had 5 EBV$^+$ BL with typical starry sky pattern and cluster 3 was enriched in EBV$^-$ BL with a typical starry sky, but also included 3 cases of EBV$^+$ BL with a typical starry sky and 2 cases of BL with a partial granulomatous reaction (Table 1). GEP of BL samples showed significant heterogeneity in the immune response functional categories (a detailed description of GEP is reported in supplemental Table 1). Interestingly, clusters 2 and 3 showed similarities and differences in GEP. Indeed, some features were exclusively linked to the presence of EBV, as shown by the differentially enriched genes in the NF-κB, JAK-STAT, and B-cell receptor signaling pathways (supplemental Figure 1A-C, respectively).

GEP and GSEA of immune-related genes among BL cases show differences in terms of cytokines, chemokines, macrophage polarization, and immune checkpoint molecules

We performed GSEA to assess the degree of association between gene signatures derived from the Kyoto Encyclopedia of Genes and Genomes (KEGG) and Reactome databases and BL cases. It is worth noting that the genes included in significant pathways were found mostly enriched in patients with BL EBV$^+$ and EBV$^-$ with starry sky pattern (supplemental Tables 1 and 2). Specifically, genes within the interleukin-4 (IL-4)/IL-13 pathway were enriched in these 2 groups, showing upregulation of *CD36* and *IL13RA2*[31,32] (supplemental Table 1). In addition, they were characterized by overexpression of *CCL17, CCL22, CCL2, CCL18, CCR1*, and *CCR4*, which are M2-related chemokines[33-35] (Figure 2A). Indeed, BL with starry sky also showed upregulation of M2 immune response genes (*CD163, LILRB1, LGALS3,* and *CSF1R*) in comparison with cluster 1 (Figure 2B).[36-39] Furthermore, our results demonstrated the enrichment of the immune exhaustion signature in BL with starry sky, both EBV$^+$ and EBV$^-$, as compared with BL with a granulomatous reaction. Specifically, our results showed the upregulation of several immune checkpoint molecules (*IRF4, PDCD1, HAVCR2/TIM3*, and *CTLA4*) (Figure 2C).[40-42] In contrast, BL with granulomatous reaction

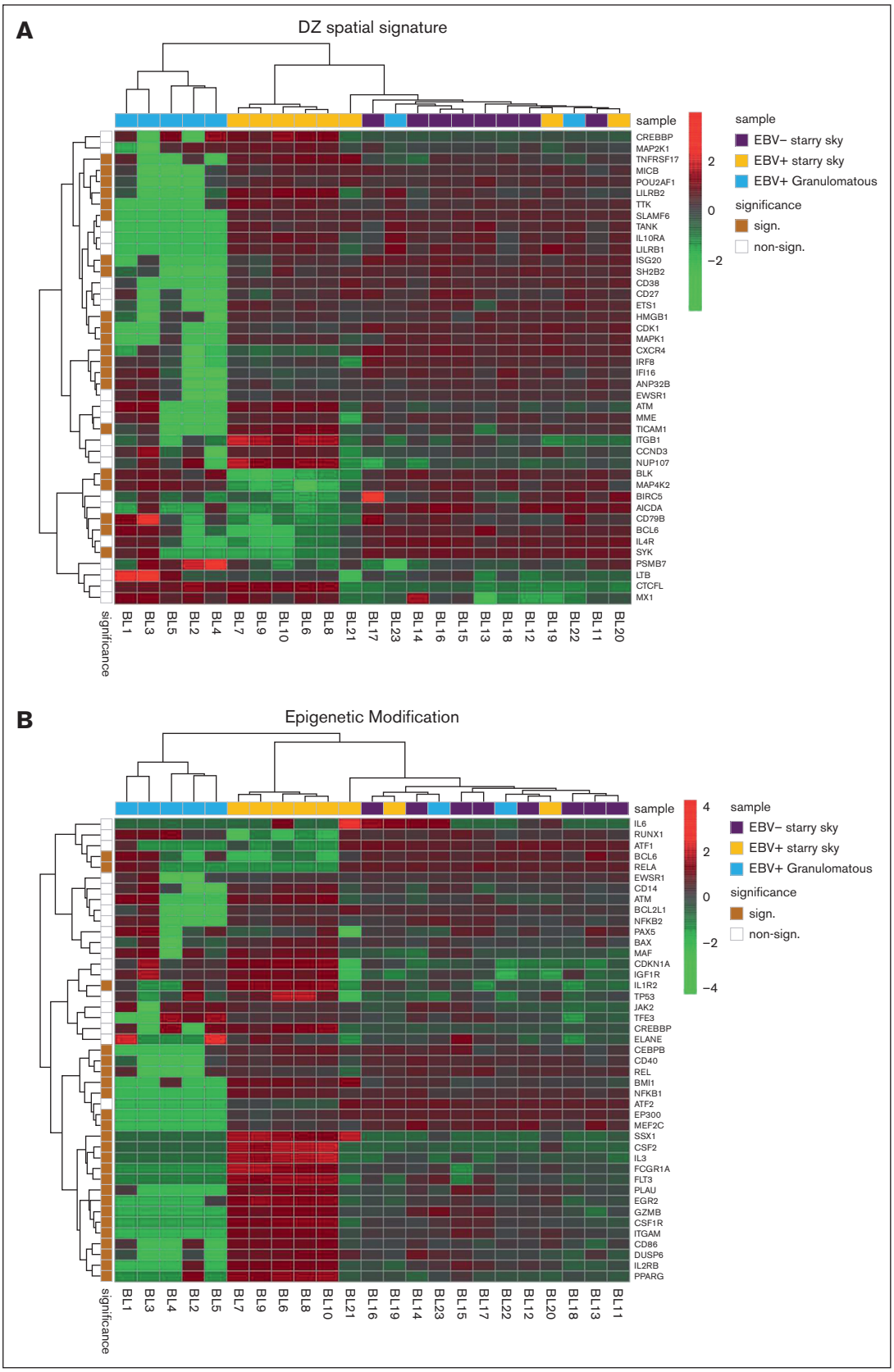

Figure 3. BL with starry sky was characterized by DZ signatures and epigenetic modification signatures. Analysis of additional signatures showed that BL with starry sky was enriched in DZ signature (A) genes and epigenetic modulation signature (B).

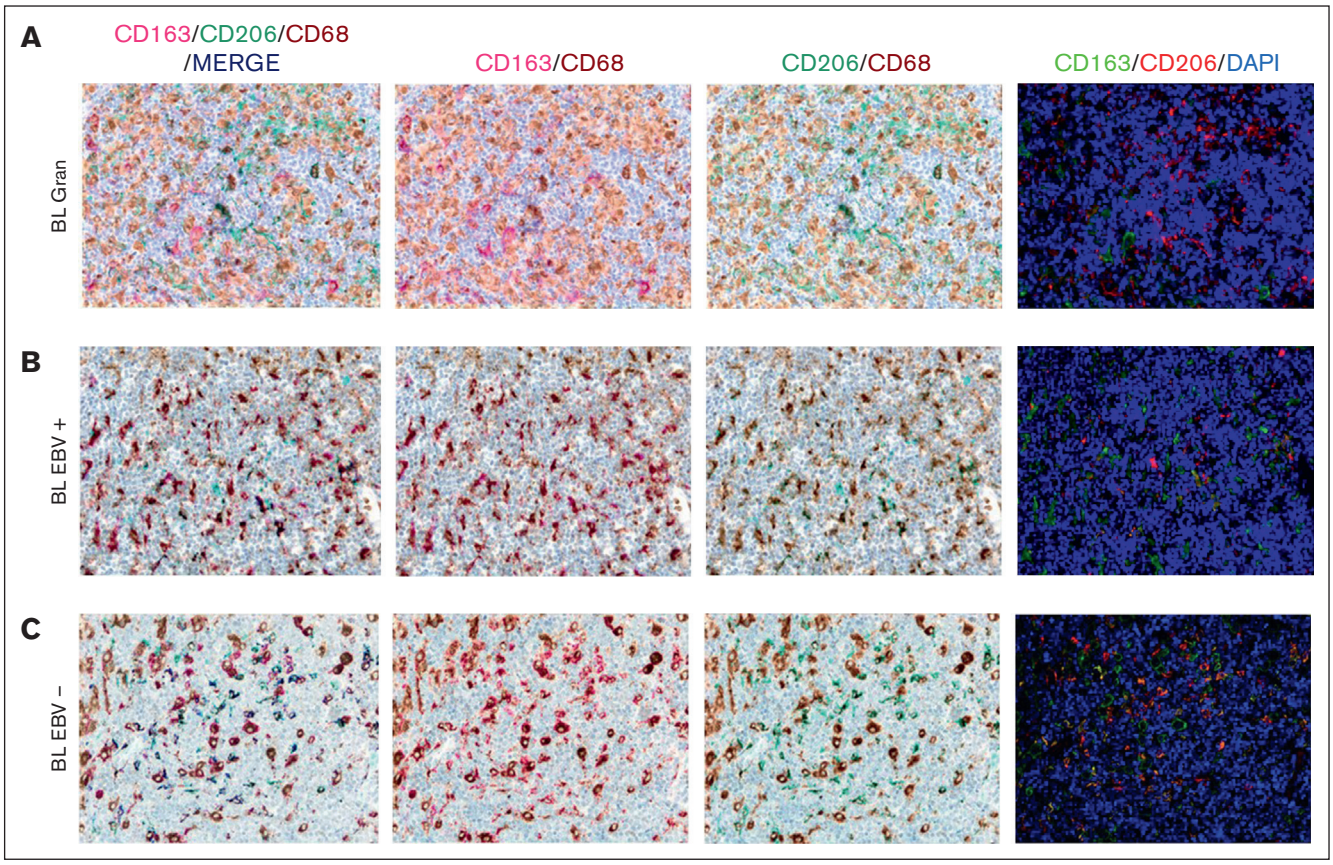

Figure 4. Multiplex immunostaining to validate M1 and M2 polarization. In BL granulomatous cases, the fraction of macrophages was significantly high, with a lower density of M2/TAM polarized macrophages (A). Conversely, BL with starry sky pattern, both EBV$^+$ (B) and EBV$^-$ (C) showed an higher density of M2 macrophages. Original magnification, ×40.

showed downregulation of all M2-related genes (*CD163, LILRB1, LGALS3, CCL17, CCL22, CCL2, CCR4, CD36,* and *IL13RA2*). Interestingly, *IRF3* and *IFNG1*, which contribute to the induction of M1 polarization, were upregulated (supplemental Table 1).[43] Because the cell of origin of BL is characterized by a dark zone (DZ) signature,[44] we considered a group of 169 DZ-UP genes differentially expressed between the DZ and LZ regions of reactive germinal centers profiled using the GeoMx Digital Spatial Profiler.[45] This new gene set identified again 3 distinct clusters. In particular, BL with starry sky pattern in both EBV$^+$ and EBV$^-$ was characterized by overexpression of DZ-expressed genes, whereas BL with granulomatous reaction showed downregulation of DZ genes. The differentially expressed genes belonged to immune evasion (*LILRB1, IRF8, ITGB1, CTCFL, MICB,* and *CD38*), M2-polarization (*LILRB2, SLAMF6, HMGB1, ATM, AICDA,* and *POU2AF1*) but also epigenetic modification (*CREBBP, ETS1, HMGB1 CDK1, EWSR, ATM,* and *SH2B2*) (Figure 3A-B).[46-61] As the epigenetic cross talk between tumor cells and TME component activates signal cascades that result in immune evasion and T-cell exhaustion, we also considered the Epigenetic Modification NanoString pathway, which reveals different expression in epigenetic modulation genes between BL with starry sky, both EBV$^+$ and EBV$^-$, and BL with granulomatous reaction. Indeed, genes involved in epigenetic modulation (*CREBBP, EP300, EWSR1,* and *ATM*)[56,59,60,62] were upregulated in BL with starry sky compared with BL with a granulomatous reaction. Finally, we performed target sequencing analysis in 3 cases of BL with granulomatous reaction for which the material was sufficient. The findings presented in supplemental Figure 2 are compared with the mutational landscape of classic BL, as reported in previous studies by us and others.[63-65] BL with granulomatous reactions exhibits a low number of mutations, and notably, lacks mutations in genes related to epigenetic mechanisms, such as *SMARC4A, ARID1A,* and *DDX3X*, which are typically found in classical BL.[64]

CIBERSORTx platform: BL with granulomatous reactions were enriched in proinflammatory cells

Focusing on the deconvolution of the gene expression data, we applied the CIBERSORTx platform to better identify the immune cell proportions. Our results revealed a high percentage of CD8 and CD4 T cells, T follicular helper cells, and M1-macrophages in BL with granulomatous as compared with BL with starry sky, which showed a high prevalence of M2-macrophages (supplemental Table 3).

Validation of GEP analysis by multiplex immunostaining

Based on the CIBERSORTx results, we decided to validate the M1 and M2 polarization and CD8$^+$ and CD4$^+$ T cells on the

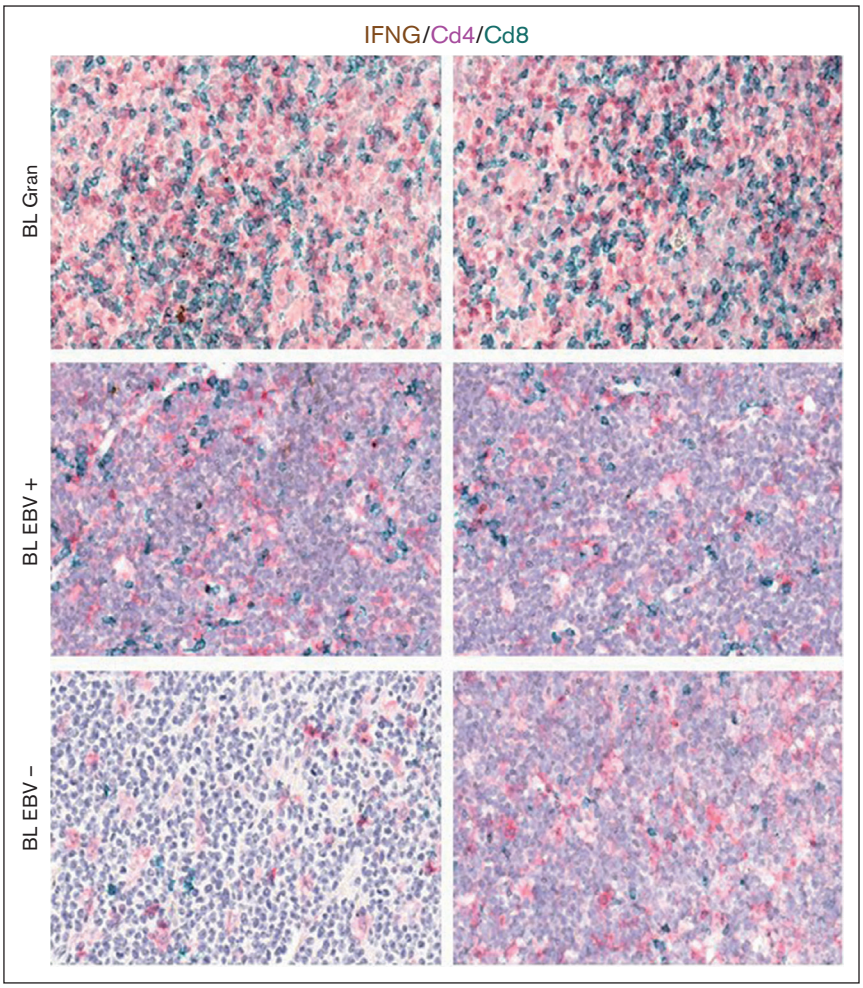

Figure 5. mRNA in situ hybridization for IFNG and immunohistochemistry (IHC) of CD4 and CD8. Representative microphotographs and quantitative analyses of mRNA in situ hybridization for IFNG and IHC for CD4 and CD8 showing the increase in the prevalence of $CD8^+$ cytotoxic lymphocytes expressing IFNG in BL case. Original magnification, ×200 and ×400.

tissue section by applying multiplex immunostaining. In situ multiplexing immunostaining for CD68 with the M2 markers CD163 and CD206 was performed in BL with granulomatous reaction and BL with starry sky. In BL with granulomatous cases, the fraction of total macrophages was significantly higher, but with a lower density of M2/TAM polarized macrophages and starry sky histiocytes (Figure 4). These results were consistent with the increased infiltration of CD4 and CD8 T cells. Indeed, to further characterize the expression of IFNG in EBV^+ BL with granulomatous reaction, we performed in situ mRNA hybridization of IFNG mRNA combined with immunohistochemistry for CD4 and CD8. Upon analyzing the results, we found that IFNG (Figure 5) was actively produced by tumor-infiltrating lymphocytes and was primarily associated with $CD8^+$ cytotoxic lymphocytes, mainly at the edges of the neoplastic cells. These results are supported by the quantitative analysis of the signals performed with HALO image analysis software and statistical analysis using PRISM (Figure 6A-B). Additionally, these cases were triple-stained for CD68, CD163, and C-Maf. Overall, in all BL with granulomatous reaction, mIF showed a prevalence of M1 macrophage defined as $CD68^+$/$CD163^-$/C-Maf^- cells, accounting for 80% to 95% of the total macrophages (supplemental Figure 5).

Discussion

The lymphoma microenvironment is a complex and dynamic network that includes immune cells, stromal cells, cytokines, blood vessels, and extracellular matrix components. The arrangement of this network is guided by neoplastic cells and can influence tumor initiation, progression, resistance to cell death, evasion from growth suppressors, and drug resistance.[66,67] Although there have been numerous studies investigating TME expression in B-cell lymphomas, there has been a limited amount of research conducted in BL.[19] Recent data using multiplex immunohistochemistry show that the TME of BL with granulomatous reaction is different, being characterized by a prevalence of M1 macrophages and proinflammatory response, which may possibly explain at times the spontaneous regression.[10] In this study, we further portrayed the immune landscape of BL using GEP with NanoString technologies, focusing on stromal cells, soluble molecules, and immune gene categories using a 730 immune-related genes panel. Our analysis led to the separation of BL into 3 clusters by GEP analysis based on immune gene categories. Cluster 1 consisted of 5 BL cases with diffuse granulomatous reaction, whereas clusters 2 and 3 were enriched of cases with BL with typical starry sky pattern, including EBV^+ or EBV^-, respectively. Some features could be linked exclusively to the presence of EBV by comparing the TME of

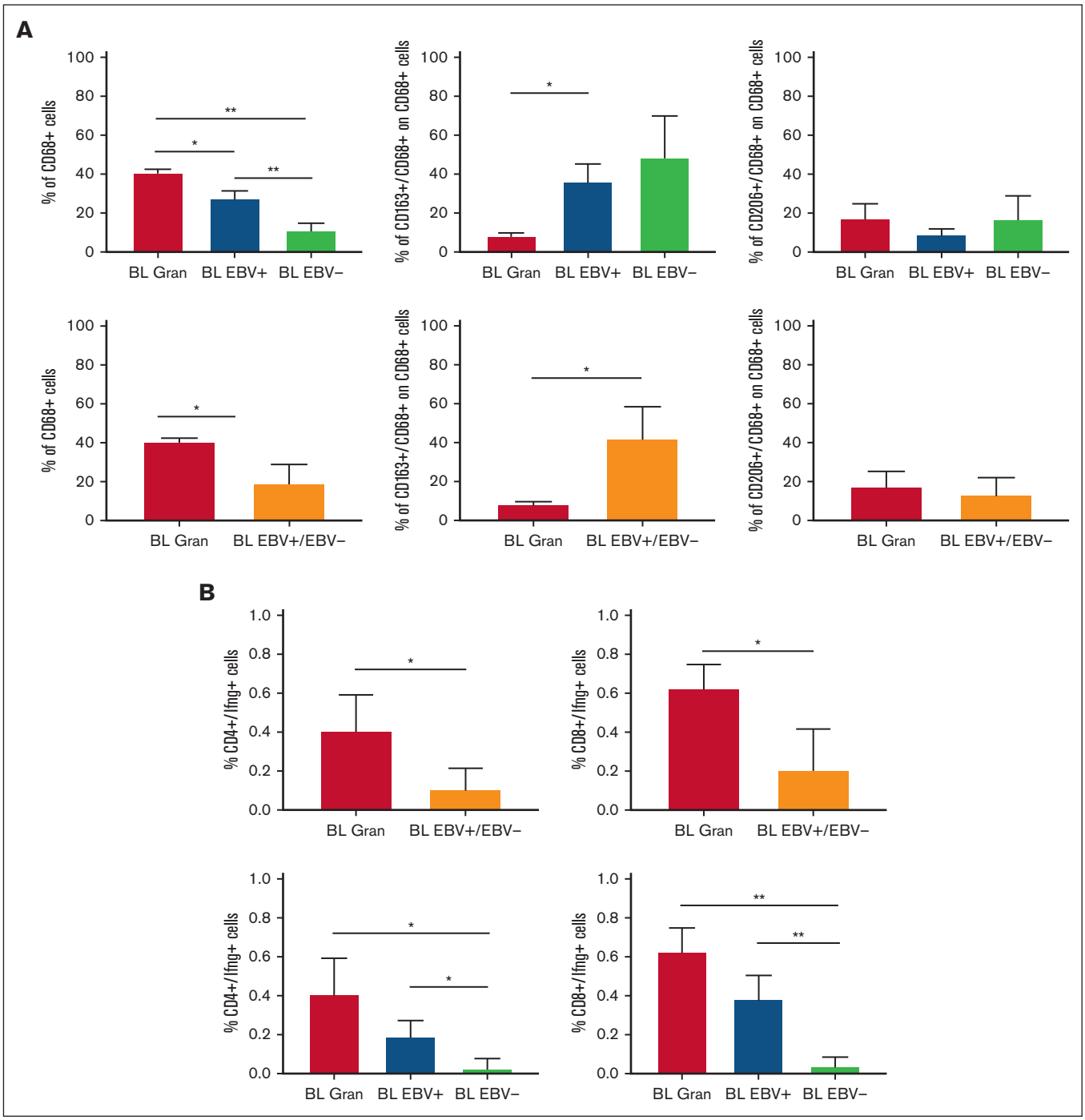

Figure 6. Quantitative analysis of immunostaining. HALO image analysis software and statistical analysis using PRISM supported the results of immunostaining (A) and combined RNAscope and IHC.

EBV$^+$ BL and EBV$^-$ BL. Indeed, our results confirm previous findings of an upregulation of the NF-κB and JAK-STAT pathways in EBV$^+$ BL, whereas a "tonic" activation of B-cell receptor signaling was more prevalent in EBV$^-$ BL.[68-74] In addition to our previous studies, here we demonstrated an increased expression of M1 genes such as *IRF3* and *INFG*, in BL with a granulomatous reaction. *IRF3* is constitutively expressed in various cell types and binds to conserved sequences known as IFN–stimulated response elements, which induce transcription of type I *IFN* genes (*IFNG1*).[74,75] By applying in situ mRNA hybridization and immunolocalization analyses, we were able to show that a fraction of effector T cells was characterized by active *IFNG* production within the inflammatory milieu of such peculiar BL cases. In particular, INFG was found to be mainly expressed in CD8$^+$ cells, suggesting its role as an effector cell in the immune response against neoplastic cells. In contrast, we demonstrated an upregulation of

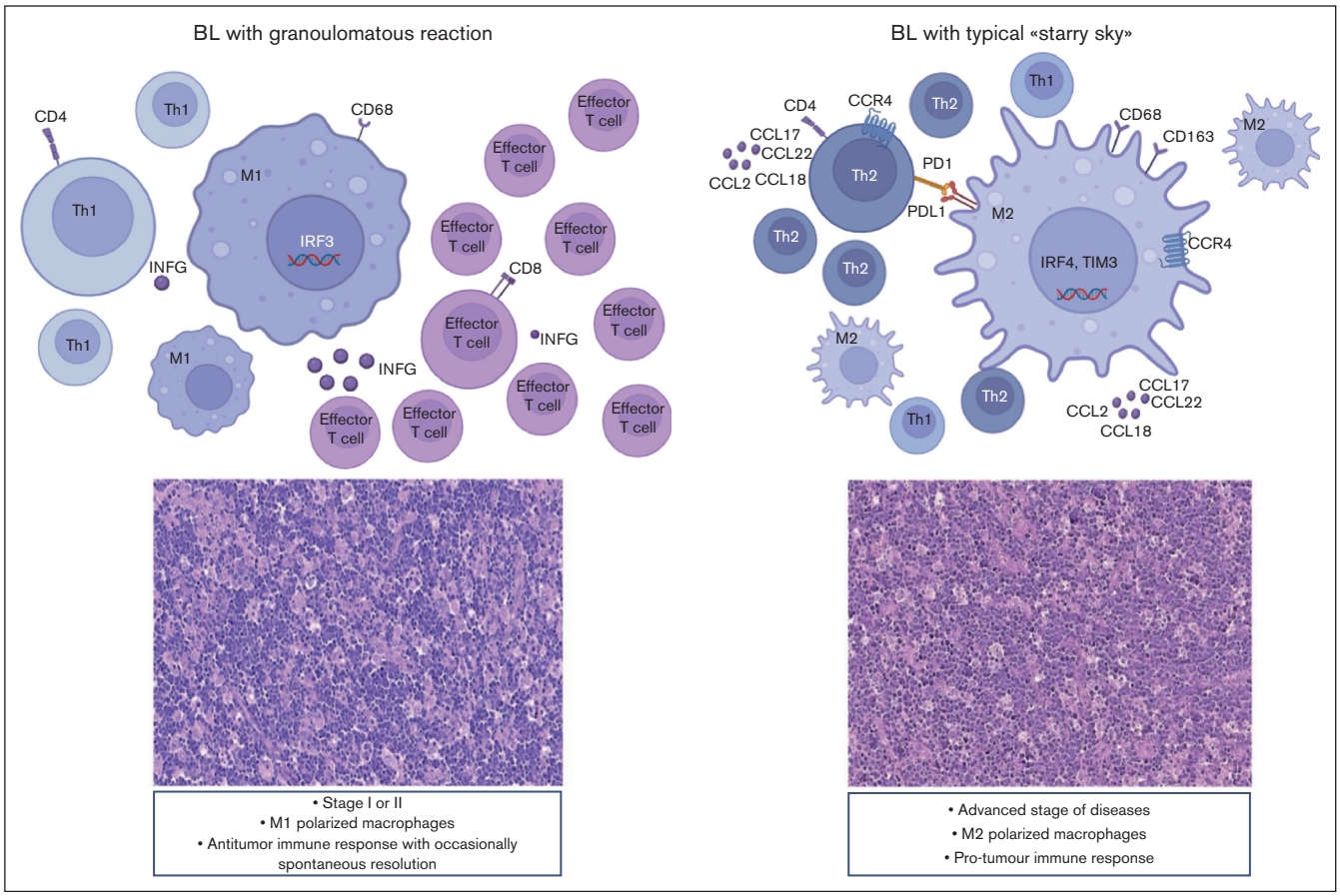

Figure 7. BL can show 2 different biological and clinical settings. M1 polarized macrophages prevail, and the immune response may be able to control neoplastic growth. In contrast, in cases characterized by the starry sky pattern, M2 macrophages dominate and may be responsible for a protumor immune response, resulting in disease rapid progression and dissemination.

the IL-4/IL-13 pathway (*CD36* and *IL13RA2*),[31,32] M2-secreted chemokines *(CCL17, CCL22, CCL2, CCR4, CCL18,* and *CCR1*),[33-35] and M2-immune response genes *(CD163, LILRB1, LGALS3,* and *CSF1R)*[36-39] in cases of BL with the typical starry sky. These results were also validated by multiplex immunostaining, which showed the prevalence of M2-macrophages in BL with starry sky associated with a low content of T cells (cold lymphomas), as compared with BL with granulomatous reaction characterized by a high proportion of M1-macrophages and reactive T lymphocytes (hot lymphomas). Intriguingly, a recent paper reported that targeting the chemokine CCL22 induces an intense granulomatous reaction and limits EBV infection from spreading in an experimental model.[40] Furthermore, here we demonstrated that BL with starry sky shows overexpression of immune checkpoint genes (*IRF4, PDCD1, HAVCR2/TIM3*, and *CTLA4*), which favors the immune escape of tumor.[41-43] These results were further confirmed by the analysis of additional signatures. In particular DZ signature genes (*CD38, CDK1, SLAMF6, CD27, TNFRSF17, MAPK1, SH2B2, CREBBP, LILRB1, EWSR1, ATM, AICDA, ETS1, HMGB1, POU2AF1, TTK, TANK,* and *IFI16*) and the epigenetic modulation signature (*CREBBP, EP300, EWSR1,* and *ATM*)[47-63,76] were upregulated in BL with starry sky both EBV^+ and EBV^-. Although these differences may be related to diverse tumor cell components, we cannot completely exclude a different cell of origin during the B-cell differentiation steps, as differences in TME-related genes, not typical of the DZ, in addition to tumor-related genes (epigenetic mechanism and metabolism) were identified.[20,77] The upregulation of the epigenetic modulation genes may activate a signal cascade that results in immune evasion and T-cell exhaustion in these cases.[78] The genetic landscape also revealed a low number of mutations and a lack of mutations in genes related to epigenetic mechanisms and immunescape in BL with granulomatous reaction. Although our data do not provide clear evidence of intrinsic differences in the tumor cells, our results revealed differences related to genes involved in both genetic and epigenetic mechanisms that are at work favoring the immunescape in BL with a starry sky pattern, both EBV^+/EBV^-.[64-66] Finally, our series showed that BL with a diffuse granulomatous reaction is typically diagnosed at an early disease stage, namely, stage I or II. Interestingly, 3 of 5 cases showed spontaneous regression, and 2 patients were in complete remission after 5 years of follow-up. In contrast, BLs with a starry sky pattern, both EBV^+ and EBV^-, were significantly associated with advanced stages of disease (stage III or IV and bulky disease). Thus, based on our results, we may envision biological-clinical settings characterized by an immune response able to control the neoplastic growth in cases with a diffuse granulomatous reaction and a protumor immune response in BL with starry sky pattern (Figure 7). The dynamic process of

macrophage plasticity may be responsible for this scenario. Novel therapeutic strategies, able to induce TAM repolarization and target epigenetic regulators, have been introduced and may have the potential to be a game-changer in the fight against BL lymphoma and improve patient outcomes, opening up alternative therapeutic avenues for patients refractory to therapy.[78,79]

Acknowledgment

This study was supported by the Associazione Italiana per la Ricerca sul Cancro 5 × 1000 grant (number 21198 [S.P.]).

Authorship

Contribution: M.C.S. designed, performed, and interpreted experiments bioinformatic analyses, and wrote the manuscript; G.B. performed and interpreted the statistical and bioinformatic analyses; M.D.C. and M.R.S. performed bioinformatic analyses; G.M. performed multiplex immunostaining and combined RNAscope and immunohistochemistry; S.T., G.B., C.I.L., E.F., B.B., F.A., R.G., and R.B. performed experiments; M.G., M.V., V.M., N.O., J.N., R.S., G.D.S., D.F., C.B., T.M., G.O., R.B., L.Q.F., F.F., P.M., C.T., S.P., S.L., and L.L. provided and analyzed the molecular and clinical data of patients with Burkitt lymphoma; S.L. and L.L. designed and supervised the experiments, analyzed the data, and wrote the manuscript; and all authors discussed the results and commented on the manuscript.

Conflict-of-interest disclosure: The authors declare no competing financial interests.

ORCID profiles: G.B., 0000-0001-7328-9675; M.R.S., 0000-0002-1078-2128; B.B., 0000-0001-9668-0925; D.F., 0009-0002-1772-3750; T.M., 0000-0003-1223-6275; L.Q.-F., 0000-0001-7156-5365; C.T., 0000-0002-0821-6231.

Correspondence: Stefano Lazzi, Department of Medical Biotechnology, Anatomical Pathology Section, University of Siena, via delle Scotte, Siena 53100, Italy; email: lazzi2@unisi.it.

References

1. Anderson NM, Simon MC. The tumor microenvironment. *Curr Biol*. 2020;30(16):R921-R925.
2. Fowler NH, Cheah CY, Gascoyne RD, et al. Role of the tumor microenvironment in mature B-cell lymphoid malignancies. *Haematologica*. 2016;101(5):531-540.
3. Scott DW, Gascoyne RD. The tumour microenvironment in B cell lymphomas. *Nat Rev Cancer*. 2014;14(8):517-534, 2014;14(8):517-534.
4. Gopal S, Gross TG. How I treat Burkitt lymphoma in children, adolescents, and young adults in sub-Saharan Africa. *Blood*. 2018;132(3):254-263.
5. Ngoma T, Adde M, Durosinmi M, et al. Treatment of Burkitt lymphoma in equatorial Africa using a simple three-drug combination followed by a salvage regimen for patients with persistent or recurrent disease. *Br J Haematol*. 2012;158(6):749-762.
6. Alaggio R, Amador C, Anagnostopoulos I, et al. The 5th edition of the World Health Organization classification of haematolymphoid tumours: lymphoid neoplasms. *Leukemia*. 2022;36(7):1720-1748.
7. Yu H, Robertson ES. Epstein–Barr virus history and pathogenesis. *Viruses*. 2023;15(3):714.
8. Ford CA, Petrova S, Pound JD, et al. Oncogenic properties of apoptotic tumor cells in aggressive B cell lymphoma. *Curr Biol*. 2015;25(5):577-588.
9. Pham LV, Pogue E, Ford RJ. The role of macrophage/B-cell interactions in the pathophysiology of B-cell lymphomas. *Front Oncol*. 2018;8:147.
10. Granai M, Mundo L, Akarca AU, et al. Immune landscape in Burkitt lymphoma reveals M2-macrophage polarization and correlation between PD-L1 expression and non-canonical EBV latency program. *Infect Agent Cancer*. 2020;15:28.
11. Murray PJ. Macrophage polarization. *Annu Rev Physiol*. 2017;79(1):541-566.
12. Xiong X, Xie X, Wang Z, Zhang Y, Wang L. Tumor-associated macrophages in lymphoma: from mechanisms to therapy. *Int Immunopharm*. 2022;112:109235.
13. Mills CD, Kincaid K, Alt JM, Heilman MJ, Hill AM. M-1/M-2 macrophages and the Th1/Th2 paradigm. *J Immunol*. 2000;164(12):6166-6173.
14. Wang N, Liang H, Zen K. Molecular mechanisms that influence the macrophage m1–m2 polarization balance. *Front Immunol*. 2014;5:614.
15. Hollingsworth HC, Longo DL, Jaffe ES. Small noncleaved cell lymphoma associated with florid epithelioid granulomatous response. A clinicopathologic study of seven patients. *Am J Surg Pathol*. 1993;17(1):51-59.
16. Haralambieva E, Rosati S, van Noesel C, et al. Florid granulomatous reaction in Epstein-Barr virus-positive nonendemic Burkitt lymphomas: report of four cases. *Am J Surg Pathol*. 2004;28(3):379-383.
17. Schrager JA, Pittaluga S, Raffeld M, Jaffe ES. Granulomatous reaction in Burkitt lymphoma: correlation with EBV positivity and clinical outcome. *Am J Surg Pathol*. 2005;29(8):1115-1116.
18. Janegová A, Janega P, Ilencíková D, Babál P. Burkitt lymphoma with unusual granulomatous reaction. A case report. *Cesk Patol*. 2011;47(1):19-22.
19. Granai M, Lazzi S, Mancini V, et al. Burkitt lymphoma with a granulomatous reaction: an M1/Th1-polarised microenvironment is associated with controlled growth and spontaneous regression. *Histopathology*. 2022;80(2):430-442.
20. Cesano A. nCounter(®) PanCancer Immune Profiling Panel (NanoString Technologies, Inc., Seattle, WA). *J Immunother Cancer*. 2015;3(3):42.
21. Law CW, Chen Y, Shi W, Smyth GK. voom: precision weights unlock linear model analysis tools for RNA-seq read counts. *Genome Biol*. 2014;15(2):R29.

22. Benjamini Y, Hochberg Y. Controlling the false discovery rate: a practical and powerful approach to multiple testing. *J Royal Stat Soc Ser B Stat Methodol*. 1995;57(1):289-300.

23. Subramanian A, Tamayo P, Mootha VK, et al. Gene set enrichment analysis: a knowledge-based approach for interpreting genome-wide expression profiles. *Proc Natl Acad Sci U S A*. 2005;102(43):15545-15550.

24. Planet E. phenoTest: tools to test association between gene expression and phenotype in a way that is efficient, structured, fast and scalable. We also provide tools to do GSEA (Gene set enrichment analysis) and copy number variation. R package version 1.50.0. Accessed 31 May 2024. https://bioconductor.org/packages/phenoTest

25. Milacic M, Beavers D, Conley P, et al. The reactome pathway knowledgebase 2024. *Nucleic Acids Res*. 2024;52(D1):D672-D678.

26. Newman AM, Steen C, Liu C, et al. Determining cell type abundance and expression from bulk tissues with digital cytometry. *Nat Biotechnol*. 2019;37(7):773-782.

27. Swift ML. GraphPad prism, data analysis, and scientific graphing. *J Chem Inf Comput Sci*. 1997;37(2):411-412.

28. R Core Team. R: A Language and environment for statistical computing. vVersion 4.0. (R packages retrieved from MRAN snapshot 2021-04-01). 2021. Accessed 31 May 2024. https://cran.r-project.org

29. Barros MH, Hauck F, Dreyer JH, Kempkes B, Niedobitek G. Macrophage polarisation: an immunohistochemical approach for identifying M1 and M2 macrophages. *PLoS One*. 2013;8(11):e80908.

30. Steele KE, Brown C. Multiplex immunohistochemistry for image analysis of tertiary lymphoid structures in cancer. *Methods Mol Biol*. 2018;1845:87-98.

31. Helming L, Winter J, Gordon S. The scavenger receptor CD36 plays a role in cytokine-induced macrophage fusion. *J Cell Sci*. 2009;122(Pt 4):453-459.

32. Junttila IS, Mizukami K, Dickensheets H, et al. Tuning sensitivity to IL-4 and IL-13: differential expression of IL-4Ralpha, IL-13Ralpha1, and gammac regulates relative cytokine sensitivity. *J Exp Med*. 2008;205(11):2595-2608.

33. Qin R, Ren W, Ya G, et al. Role of chemokines in the crosstalk between tumor and tumor-associated macrophages. *Clin Exp Med*. 2023;23(5):1359-1373.

34. Chen J, Zhao D, Zhang L, et al. Tumor-associated macrophage (TAM)-derived CCL22 induces FAK addiction in esophageal squamous cell carcinoma (ESCC). *Cell Mol Immunol*. 2022;19(9):1054-1066.

35. Parisi L, Gini E, Baci D, et al. Macrophage polarization in chronic inflammatory diseases: killers or builders? *J Immunol Res*. 2018;2018:8917804.

36. Buechler C, Ritter M, Orsó E, Langmann T, Klucken J, Schmitz G. Regulation of scavenger receptor CD163 expression in human monocytes and macrophages by pro- and antiinflammatory stimuli. *J Leukoc Biol*. 2000;67(1):97-103.

37. Zhang Y, Wang H, Xu X, et al. Poor prognosis and therapeutic responses in LILRB1-expressing M2 macrophages-enriched gastric cancer patients. *Front Oncol*. 2021;11:668707.

38. Jia W, Kidoya H, Yamakawa D, Naito H, Takakura N. Galectin-3 accelerates M2 macrophage infiltration and angiogenesis in tumors. *Am J Pathol*. 2013;182(5):1821-1831.

39. Cannarile MA, Weisser M, Jacob W, Jegg AM, Ries CH, Rüttinger D. Colony-stimulating factor 1 receptor (CSF1R) inhibitors in cancer therapy. *J Immunother Cancer*. 2017;5(1):53.

40. Maroui MA, Odongo GA, Mundo L, et al. Aflatoxin B1 and Epstein-Barr virus-induced CCL22 expression stimulates B cell infection. *Proc Natl Acad Sci U S A*. 2024;121(16):e2314426121.

41. Lu J, Liang T, Li P, Yin Q. Regulatory effects of IRF4 on immune cells in the tumor microenvironment. *Front Immunol*. 2023;14:1086803.

42. Buchbinder EI, Desai A. CTLA-4 and PD-1 pathways: similarities, differences, and implications of their inhibition. *Am J Clin Oncol*. 2016;39(1):98-106.

43. Sauer N, Janicka N, Szlasa W, et al. TIM-3 as a promising target for cancer immunotherapy in a wide range of tumors. *Cancer Immunol Immunother*. 2023;72(11):3405-3425.

44. Yanai H, Chiba S, Hangai S, et al. Revisiting the role of IRF3 in inflammation and immunity by conditional a n d specifically targeted gene ablation in mice. *Proc Natl Acad Sci U S A*. 2018;115(20):5253-5258.

45. Loeffler-Wirth H, Kreuz M, Schmidt M, Ott G, Siebert R, Binder H. Classifying germinal center derived lymphomas–navigate a complex transcriptional landscape. *Cancers*. 2022;14(14):3434.

46. L'Imperio V, Morello G, Vegliante MC, et al. Spatial transcriptome of a germinal center plasmablastic burst hints at MYD88/CD79B mutants-enriched diffuse large B-cell lymphomas. *Eur J Immunol*. 2022;52(8):1350-1361.

47. Nixon BG, Kuo F, Ji L, et al. Tumor-associated macrophages expressing the transcription factor IRF8 promote T cell exhaustion in cancer. *Immunity*. 2022;55(11):2044-2058.e5.

48. Xu C, Xie XL, Kang N, Jiang HQ. Evaluation of ITGB1 expression as a predictor of the therapeutic effects of immune checkpoint inhibitors in gastric cancer. *BMC Gastroenterol*. 2023;23(1):298.

49. Oreskovic E, Wheeler EC, Mengwasser KE, et al. Genetic analysis of cancer drivers reveals cohesin and CTCF as suppressors of PD-L1. *Proc Natl Acad Sci U S A*. 2022;119(7):e2120540119.

50. Ferrari de Andrade L, Kumar S, Luoma AM, et al. Inhibition of MICA and MICB shedding elicits NK- cell-mediated immunity against tumors resistant to cytotoxic T cells. *Cancer Immunol Res*. 2020;8(6):769-780.

51. Chen L, Diao L, Yang Y, et al. CD38-mediated immunosuppression as a mechanism of tumor cell escape from PD-1/PD-L1 blockade. *Cancer Discov*. 2018;8(9):1156-1175.
52. Chen HM, van der Touw W, Wang YS, et al. Blocking immunoinhibitory receptor LILRB2 reprograms tumor-associated myeloid cells and promotes antitumor immunity. *J Clin Invest*. 2018;128(12):5647-5662.
53. Meng Q, Duan X, Yang Q, et al. SLAMF6/Ly108 promotes the development of hepatocellular carcinoma via facilitating macrophage M2 polarization. *Oncol Lett*. 2022;23(3):83.
54. Son M, Porat A, He M, et al. C1q and HMGB1 reciprocally regulate human macrophage polarization. *Blood*. 2016;128(18):2218-2228.
55. Teater M, Dominguez PM, Redmond D, et al. AICDA drives epigenetic heterogeneity and accelerates germinal center-derived lymphomagenesis. *Nat Commun*. 2018;9(1):222.
56. Song S, Cao C, Choukrallah MA, et al. OBF1 and Oct factors control the germinal center transcriptional program. *Blood*. 2021;137(21):2920-2934.
57. Hashwah H, Schmid CA, Kasser S, et al. Inactivation of CREBBP expands the germinal center B cell compartment, down-regulates MHCII expression and promotes DLBCL growth. *Proc Natl Acad Sci U S A*. 2017;114(36):9701-9706.
58. Luchtel RA, Zhao Y, Aggarwal RK, Pradhan K, Maqbool SB. ETS1 is a novel transcriptional regulator of adult T-cell leukemia/lymphoma of North American descent. *Blood Adv*. 2022;6(20):5613-5624.
59. Dai Y, Jin F, Wu W, Kumar SK. Cell cycle regulation and hematologic malignancies. *Blood Sci*. 2019;1(1):34-43.
60. Lee J, Nguyen PT, Shim HS, et al. EWSR1, a multifunctional protein, regulates cellular function and aging via genetic and epigenetic pathways. *Biochim Biophys Acta, Mol Basis Dis*. 2019;1865(7):1938-1945.
61. Abraham RT. Checkpoint signaling: epigenetic events sound the DNA strand-breaks alarm to the ATM protein kinase. *Bioessays*. 2003;25(7):627-630.
62. Wakioka T, Sasaki A, Mitsui K, et al. APS, an adaptor protein containing Pleckstrin homology (PH) and Src homology-2 (SH2) domains inhibits the JAK-STAT pathway in collaboration with c-Cbl. *Leukemia*. 1999;13(5):760-767.
63. Zhu Y, Wang Z, Li Y, et al. The Role of CREBBP/EP300 and its therapeutic implications in hematological malignancies. *Cancers*. 2023;15(4):1219.
64. Abate F, Ambrosio MR, Mundo L, et al. Distinct viral and mutational spectrum of endemic Burkitt lymphoma. *PLoS Pathog*. 2015;11(10):e1005158.
65. Grande BM, Gerhard DS, Jiang A, et al. Genome-wide discovery of somatic coding and noncoding mutations in pediatric endemic and sporadic Burkitt lymphoma. *Blood*. 2019;133(12):1313-1324.
66. Love C, Sun Z, Jima D, et al. The genetic landscape of mutations in Burkitt lymphoma. *Nat Genet*. 2012;44(12):1321-1325.
67. Mulder TA, Wahlin BE, Österborg A, Palma M. Targeting the immune microenvironment in lymphomas of B-cell origin: from biology to clinical application. *Cancers*. 2019;11(7):915.
68. Rohde M, Bonn BR, Zimmermann M, et al. Relevance of ID3-TCF3-CCND3 pathway mutations in pediatric aggressive B-cell lymphoma treated according to the non-Hodgkin lymphoma Berlin- Frankfurt-Münster protocols. *Haematologica*. 2017;102(6):1091-1098.
69. Poirel HA, Ambrosio MR, Piccaluga PP, Leoncini L. Pathology and molecular pathogenesis of Burkitt lymphoma and lymphoblastic lymphoma. In: Lenz G, Salles G, eds. *Aggressive Lymphomas. Hematologic Malignancies*. 1st ed. Springer International publishing; 2018:75-94.
70. Piccaluga PP, De Falco G, Kustagi M, et al. Gene expression analysis uncovers similarity and differences among Burkitt lymphoma subtypes. *Blood*. 2011;117(13):3596-3608.
71. Nepomuceno RR, Snow AL, Robert Beatty P, Krams SM, Martinez OM. Constitutive activation of Jak/STAT proteins in Epstein-Barr virus-infected B-cell lines from patients with posttransplant lymphoproliferative disorder. *Transplantation*. 2002;74(3):396-402.
72. Chen L, Monti S, Juszczynski P, et al. SYK-dependent tonic B-cell receptor signaling is a rational treatment target in diffuse large B-cell lymphoma. *Blood*. 2008;111(4):2230-2237.
73. Seda V, Mraz M. B-cell receptor signalling and its crosstalk with other pathways in normal and malignant cells. *Eur J Haematol*. 2015;94(3):193-205.
74. Upadhyay R, Hammerich L, Peng P, Brown B, Merad M, Brody JD. Lymphoma: immune evasion strategies. *Cancers*. 2015;7(2):736-762.
75. Günthner R, Anders HJ. Interferon-regulatory factors determine macrophage phenotype polarization. *Mediators Inflamm*. 2013;2013:731023.
76. Tripodo C, Zanardi F, Iannelli F, et al. A spatially resolved dark- versus light-zone microenvironment signature subdivides germinal center-related aggressive B cell lymphomas. *iScience*. 2020;23(10):101562.
77. Ambrosio MR, Lo Bello G, Amato T, et al. The cell of origin of Burkitt lymphoma: germinal centre or not germinal centre? *Histopathology*. 2016;69(5):885-886.
78. Andreescu M. Epigenetic alterations that are the backbone of immune evasion in T-cell malignancies. *Cureus*. 2024;16(1):e51662.
79. van Dalen FJ, van Stevendaal MHME, Fennemann FL, Verdoes M, Ilina O. Molecular repolarisation of tumour-associated macrophages. *Molecules*. 2018;24(1):9.